

Entropy measures as indicators of connectivity paths in the human brain

Ania Mesa-Rodríguez, Ernesto Estevez-Rams and Holger Kantz
*Universidad de La Habana, San Lazaro y L. CP 10400. La Habana. Cuba. Max Planck
Institute for the Physics of Complex Systems. Nöthnitzer Strasse 38. D-01187 Dresden*

How does the information flow between different brain regions during various stimuli? This is the question we aim to address by studying complex cognitive paradigms in terms of Information Theory. To assess creativity and the emergence of patterns from a Shannon perspective, we applied a range of tools including Entropy Density, Effective Measure Complexity, and the Lempel-Ziv distance. These entropic tools enable the detection of both linear and non-linear dynamics without relying on pre-established parameters, models, or prior assumptions about the data. To identify connections between different brain regions, we analyze task-based fMRI data from subjects during motor, working memory, emotion recognition, and language stimuli to gain insight into these complex cognitive processes. Since this method does not depend on prior knowledge, it is particularly well-suited for exploratory research and facilitates the discovery of previously unidentified connections or patterns in the brain. The capacity to identify non-linear dynamics is especially important for studying brain connectivity, as the brain exhibits significant non-linear interactions across multiple functional levels.

I. INTRODUCTION

The topological and functional complexity of the brain is a crucial aspect of its operation; its ability to encode information is not limited to a single scale, ranging from macroscopic to microscopic levels¹. Although a neuron is considered the primary computational unit essential for brain function at the microscale, cortical columns composed of anatomically or functionally distinct neuronal populations represent the minimal intelligent units capable of performing logical operations at the mesoscopic scale, which is closely related to noninvasive recordings². At the macroscopic level, techniques such as fMRI and structural MRI provide insights into whole-brain organization, large-scale networks, and functional specialization in areas of the brain. Recent studies have attempted to bridge the multiple scales of organization into an integrative theory, finding consistent organizational principles of connectivity at both the macroscale and the neuronal levels^{3,4}.

The human connectome represents the intricate network of structural and functional connections between different regions and areas of the brain, providing crucial insights into how these regions are interconnected and communicate. This understanding is fundamental to unraveling brain function, including processes such as cognition, perception, emotion, and memory. Mapping the connectome can help identify abnormal connectivity patterns associated with conditions such as Alzheimer's disease^{5,6}, Parkinson⁷, schizophrenia, ataxia, autism, and traumatic brain injuries⁸. This knowledge is vital for diagnosis, treatment, and potential interventions. In fMRI measurements, when performing attention-demanding cognitive tasks, a change in the response of different regions is observed, some signaling increase in activity, some a decrease of activity and some remain more or less indifferent⁹⁻¹².

When analyzing fMRI data different approaches have been used to infer direct interactions between brain regions through various methods, including causal models^{13,14}, Granger causality¹⁵, Spectral measures¹⁶, partial directed coherence¹⁷, graph theory¹⁸, community detection¹⁹, among others.

In this work we propose a new approach to analyze cognitive states aimed at detecting both linear and non-linear dynamics without relying on parameters, models, or correct prior knowledge of the network. We tested the method on fMRI data extracted from the Human Connectome Project²⁰. Task-based fMRI time series signals of subjects during diverse stimuli, including motor, emotion, working memory, and language tasks were used.

The tools are based on Shannon entropy but instead of relying solely on the entropy density, as done before^{21,22}, we applied a range of information theory tools, including entropy density, effective measure complexity, and informational distance in a combined way, to assess creativity and the emergence of patterns. Notably, these entropic tools allow for the detection of both linear and non-linear dynamics without relying on pre-established parameters, models, or prior assumptions about the data. The ability to detect non-linear dynamics is particularly relevant for analyzing brain connectivity, as the brain exhibits strong non-linear interactions across different levels of function²³. Since this approach does not require prior knowledge, it is ideal for exploratory research and helps uncover previously unknown connections or behaviors in the brain.

The entropy density, h , which is also known as the entropy rate or Kolmogorov-Sinai entropy depending on the field, is a measure of randomness in a signal measured by the signal's ability to create new patterns²⁴; while the structure has been assessed by the effective measure complexity, E , also known as excess entropy, which is related to the persistence of patterns, or memory of a system^{25,26}. Studying written language through entropy markers, entropy density has been used as a measure of creativity in the sense of the capacity of a system to create information or new patterns,

while effective measure complexity captures the redundancy of a signal, and, in the case of language, has proven useful in grasping this characteristic at all length scales in a single parameter²⁷. The hallmark of complexity lies between full randomness, or maximum entropy density value, on one side, and complete predictability or zero entropy density on the other. When analyzing the signals coming from the brain regions, one hopes that their complex behavior can be captured, at least partially, by the tuple (h, E) , and that is the hypothesis tested in this work. Furthermore, an additional magnitude, informational distance, d , could become relevant when studying functional connections between regions, as it measures how distant one signal is from another in terms of one reproducing the patterns of the other while, possibly, generating their own independent behavior.

II. METHODS

Data acquisition. Task-based fMRI time series taken from the Human Connectome Project data server²⁰ was used for five types of exercises: resting state, motor, working memory, emotion, and language; details can be found in Wu et. al²⁸.

During resting-state fMRI (rfMRI) scans, participants kept their eyes open, maintaining a relaxed fixation on a bright cross-hair projected onto a dark background in a dark room.

For the motor task, participants received visual cues instructing them to either tap their left or right fingers, squeeze their left or right toes, or move their tongue. Each movement block lasted 12 seconds (consisting of 10 movements) and was preceded by a 3-second visual cue. Across two runs, there were 13 blocks, including 2 blocks of tongue movements, 4 blocks of hand movements (2 right and 2 left), and 4 blocks of foot movements (2 right and 2 left). Additionally, each run included 3 fixation blocks of 15 seconds.

In the working memory exercise, participants were shown blocks of trials featuring images of places, tools, faces, and body parts (non-mutilated and non-nude). During each run, these four types of stimuli were presented in separate blocks; half of the blocks involved a 2-back working memory task, and the other half used a 0-back task as a comparison for working memory performance. At the start of each block, a 2.5-second cue indicated the task type (and the target for the 0-back task). Each of the two runs included 8 task blocks (comprising 10 trials of 2.5 seconds each, lasting 25 seconds per block) and 4 fixation blocks (lasting 15 seconds). For each trial, the stimulus was displayed for 2 seconds, followed by a 500 ms inter-task interval (ITI).

In the emotion task, participants are shown blocks of trials where they are asked to either identify which of two faces at the bottom of the screen matches the face at the top, or which of two shapes at the bottom matches the shape at the top. The faces display either an angry or fearful expression. The trials are grouped into blocks of 6 trials focused on either faces or shapes. Each stimulus is shown for 2000 ms, followed by a 1000 ms inter-trial interval. Before each block, a 3000 ms cue indicates whether the task is "shape" or "face," making the total block duration 21 seconds, including the cue. Each of the two runs contains 3 face blocks and 3 shape blocks, with 8 seconds of fixation at the end of each run.

Finally, the language task involves two runs, each alternating between 4 blocks of a story task, and 4 blocks of a math task. The block lengths vary, averaging around 30 seconds, but the math blocks are designed to match the length of the story blocks, with some additional math trials at the end of the task if needed to complete the 3.8-minute duration. In the story blocks, participants listen to short auditory stories (5-9 sentences) followed by a two-choice question that tests their understanding of the story's theme. The math task also presents auditory trials where participants are asked to solve addition or subtraction problems. Each trial presents a series of arithmetic operations followed by two choices for selecting the correct answer. The math task is adaptive, adjusting the difficulty level to maintain consistent challenge across participants.

The data was pre-processed through the Human Connectome Project standard pre-processing pipeline, which ensures that the fMRI data is cleaned and standardized, making it suitable for analysis. This pipeline includes essential steps such as motion correction to reduce distortions caused by participant movement during scanning, removal of noise and artifacts, alignment to a standard brain template to ensure that brain regions are consistently mapped across subjects, spatial smoothing, and temporal filtering, among others (Details can be found in Wu et. al.²⁸).

The brain was parcelled into Regions of Interest (ROIs) using the Glasser atlas²⁹, which is known for its high-resolution definition of cortical areas. This parcellation step divides the brain into 360 distinct regions. The first 180 regions correspond to the left hemisphere, while the remaining 180, from ROIs 180 to 360, represent their homologous region in the right hemisphere.

Data preprocessing. fMRI measures the Blood Oxygenation Level-Dependent (BOLD) signal, which reflects changes in blood oxygen levels. The principle behind it is that when a brain region becomes active, it consumes more oxygen and glucose, leading to increased blood flow to that area. This change is detected by MRI due to the magnetic properties of deoxyhemoglobin. (Figure 1).

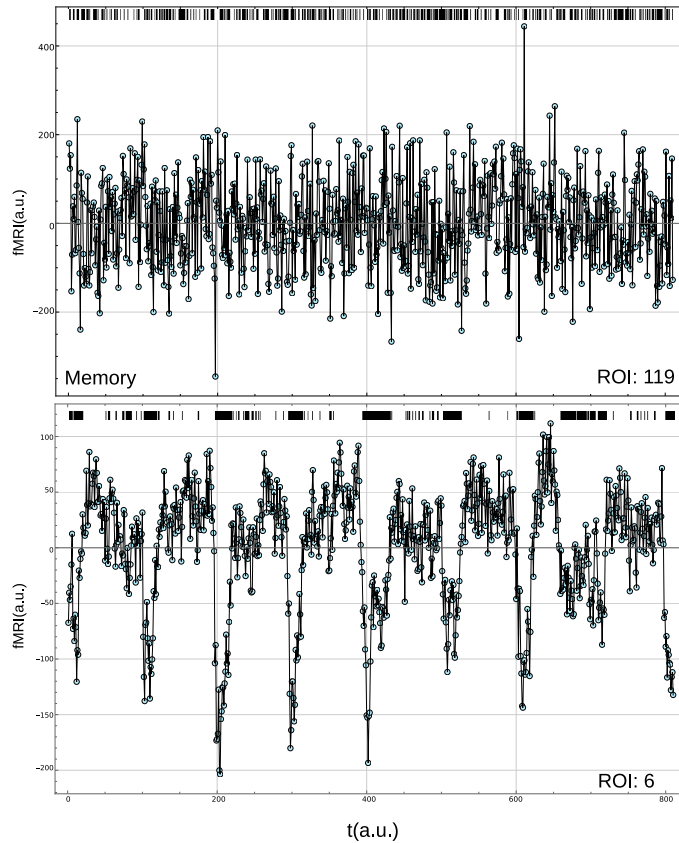


FIG. 1: **fMRI signal.** Blood oxygenation level-dependent (BOLD) signal from the fMRI measurement of (upper) inactive region, and (lower) active region of the brain. Binarization (black-and-white bar over the signal plot) is performed using the mean value as a threshold. The binary sequence shows as a time series if the signal is below (0) or above (1) the threshold value, which can be related, referred to as the baseline, to the higher or lower oxygen content of the region, in turn indirectly related to the region's activity.

Before the entropic measures are applied, the data needs to be discretized. For each time series, the mean value is computed and used as a threshold for binarization. Binarization is a drastic procedure resulting in the loss of information from the original signal. What is hoped for is that the binary sequence still carries enough information to grasp relevant features of the dynamics of the system. If this is the case, it can only be asserted by the results themselves, as will be discussed below.

The binary sequence can be understood as follows. Taking the mean value as a baseline reference, the signal space has been segmented into two regions, above and below the baseline. A change of values $1 \Leftrightarrow 0$ means crossing from one region to the other. Patterns in the binary sequence, therefore, are to be understood in terms of this crossing. Any variation of the signal within one of the two regions is lost in the discretization process (Figure 1).

Entropic measures. Three main entropic based magnitudes will be used in the study: entropy density, effective measure complexity and information distance.

Entropy density has been defined in several equivalent ways; the entropy density is related to the rate of change of the Shannon block entropy with a time series length²⁴.

$$h_\mu = \lim_{L \rightarrow \infty} \frac{H(L)}{L}, \quad (1)$$

where $H(L) = -\sum p(s^L) \log p(s^L)$ is the block entropy over the probabilities $p(s^L)$ of a given subsequence s^L of length L in the time series. Summation is made over all possible sequences of length L ²⁴. Entropy density measures the amount of randomness or unpredictability when observing an infinitely long time series. We estimate the entropy density through the Lempel-Ziv factorization (See supplementary information), which has been proven to be a robust estimate even for short sequences³⁰. The estimated entropy density will be denoted by h_{LZ} .

Effective measure complexity is the mutual information between the two halves of a (infinite) time series²⁵. In this

sense, it conveys the amount of information that one half has on the other half and therefore, measures correlations (memory) at all length scales without the need to assume linear behavior. Estimation of effective measure complexity is in general a difficult task²⁶, if it is assumed that the time series has finite memory and can be taken as stochastic, then a used related magnitude, which will be called LZ-effective complexity, is based on the random shuffling of the data (See supplementary materials and^{31,32}), this is the estimate used in this report and will be denoted by E_{LZ} .

The information distance³³ between two sequences S and Q , is defined as follows

$$d_{NID}(S, Q) = \frac{K(SQ) - \min\{K(S), K(Q)\}}{\max\{K(S), K(Q)\}} \quad (2)$$

where $K(S)$ represents the Kolmogorov complexity³⁴ of the time series S , which is the length of the shortest program that generates the sequence S ³⁴. SQ denotes the concatenation of both sequences. d_{NID} is normalized between 0 and 1, the latter taken as the largest attainable distance between the compared time series. The information distance does not measure how the two sequences differ point by point, it is not a Hamming type distance; instead, it quantifies their informational similarity, determining the degree of correlation between them from an algorithmic perspective: it reflects the shortest program length required to transform one sequence into the other, capturing how much new information is needed to describe one sequence in terms of the other. A practical alternative is also necessary for this distance metric, the usual procedure has been to use compression algorithms to estimate the Kolmogorov Complexities involved in the use of equation (2). Instead, in this research, an estimate of the Kolmogorov randomness will be done with the Lempel-Ziv factorization as described in³⁵ (see also supplementary material) and will be called LZ-distance and denoted by d_{LZ} .

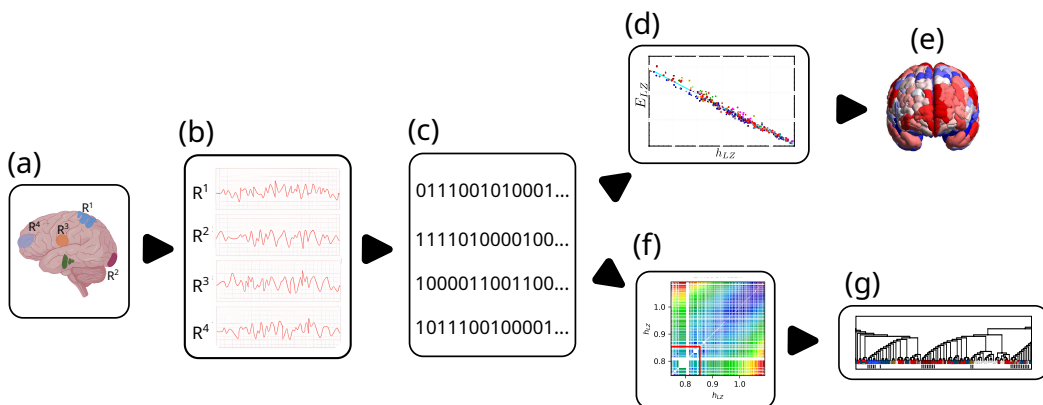


FIG. 2: **Analysis pipeline.** (a) The brain was divided into Regions of Interest (ROIs), and (b) the time series from the fMRI measurements of each region were (c) discretized and further analyzed using entropic measures, resulting in (d) the complexity-entropy maps of the task from where the (e) activated regions of the brain are determined. (f) The distance matrix between each pair of regions is computed, and the resulting (g) dendrogram of the region's distances is drawn.

Analysis pipeline. The analysis followed in our study is depicted in Figure 2: Under a given task, the fMRI signal from different regions of the brain according to Glasser parcellation is binarized; the entropic magnitudes from each resulting discrete sequence is estimated and the E_{LZ} vs h_{LZ} , complexity-entropy, map is built, the activated regions of the brain are determined from the map. For every two regions of the brain, the informational distance d_{LZ} is computed, and a distance matrix is built; the distance map allows the building of the distance dendrogram.

III. RESULTS

Figure 1 is typical of the active (lower plot) and non-active (upper plot) brain regions. There is a clear difference between the two plots, and that is what we capture by using the entropy magnitudes. The complexity-entropy map plots the relationship between entropy density and LZ-effective complexity for all brain regions involved in the experiment, as illustrated in Figure 3. Each dot represents a (h_{LZ}, E_{LZ}) tuple for one of the 360 ROIs. All values of entropy density h_{LZ} , in all tasks, are above 0.6 bit/symbol, which implies that none of the regions have a completely predictable or completely unpredictable dynamic. At the same time, the LZ-effective complexity is always above 0.45 bits/symbol, which means that some pattern formation is present on the fMRI signal. Both behaviors are common conditions for complex dynamics.

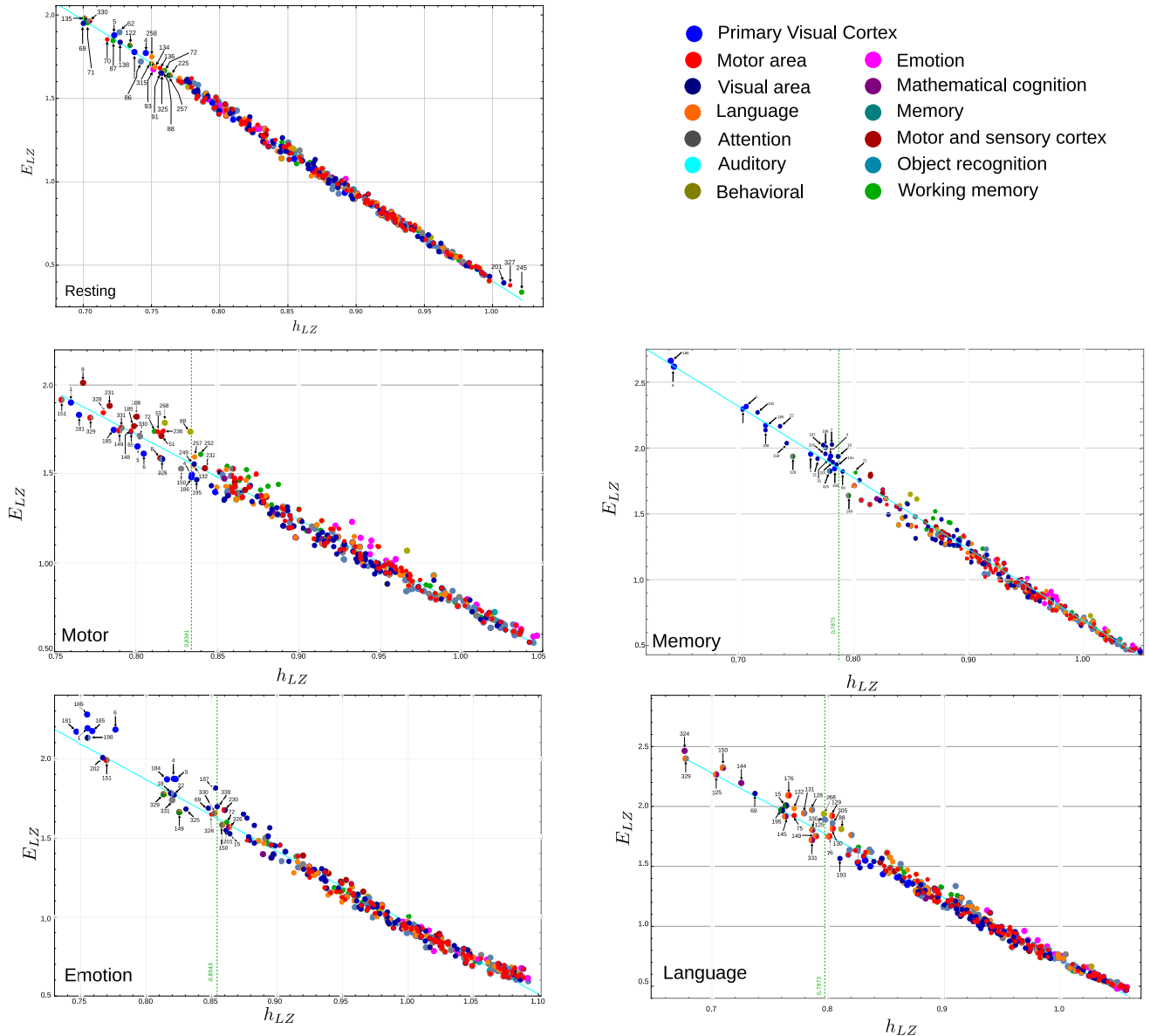


FIG. 3: **Complexity-entropy maps.** LZ-effective complexity (E_{LZ}) vs LZ-entropy density (h_{LZ}) of all regions during Resting State and in the 4 tasks: Motor, Memory, Emotion, and Language. The active regions during each task present lower h_{LZ} and higher E_{LZ} , which points to less unpredictability and more patterned behavior than the rest of the regions. The results confirm that inactive regions have higher randomness as they do not suppress the noisy background³⁶. The vertical line divides active from non-active areas. The criteria to select that threshold was based on the maximum error observed when fitting the dots, with ten neighbors, to a linear curve. This error indicates the point where the scatter significantly deviates from the line on average. Some regions previously reported as active for each task here appear as less active; that is the case in the motor task for some pre-motor areas (green dots) and motor areas (red dots) that are well below the threshold line.

For all tasks, there is a linear trend in the data, with a larger dispersion of values for low h_{LZ} and higher E_{LZ} . A least squares fit allows us to determine the residuals with respect to the fitted line. From the plot of the residuals, a threshold can be computed by taking for each point, the mean value of its 10 h_{LZ} neighbors and using as threshold the maximum value (See Supplementary Material). The threshold splits the entropy map into two regions: one with lower (larger) values of h_{LZ} (E_{LZ}) and one with larger (lower) values of the same magnitude. According to previous studies³⁶ the inactive regions do not suppress background noise, and therefore, their signal tends to appear more random; we take the lower entropy side (left of the vertical threshold line) to correspond to activated regions. For all tasks, on the active side, there are far fewer regions than on the non-active side.

Certain regions show specialized activity for different stimuli as reported in previous studies³⁷, and we will follow

those findings to understand the complexity-entropy maps.

For the motor task, 8.61% of the regions are active, namely: 1(181), 5(185), 6(186), 8(188), 9(189), 51(231), 56(236), 69, 72, 88(268), 148(328), 149(329), 150(330), 151(331), 325. The regions with lower entropy density are region PGs (ROI **151**) and Primary Visual Cortex or V1 (ROI **1**) very near its hemisphere contrapart ROI **181**. The first of these areas (ROI **151**) activates when individuals shift their visuospatial attention from one location to another, specifically in response to biological motion³⁸, whilst the other areas (ROI **1** and **181**) are the most important areas during visual activity³⁷. The area with the largest E_{LZ} value is area 3b, the Primary Sensory Cortex (ROI **9** and **189**) which receives information related to bilateral tactile stimulation, this area has been reported to work in conjunction with area 1 (ROI **231**) primarily involved in processing tactile stimuli³⁹, which is also within the four regions with the largest LZ-effective complexity values E_{LZ} . The motor task asked for a motor reaction to a visual cue.

For the motor task, all active regions identified with the Primary and Sensory Motor Cortex (ROIs **188, 9, 189, 51, 231, 52, 232, 53, 233**) lie above the fitted line, except for the Primary Motor Cortex or area 4 of the left hemisphere (ROI **8**) which lies below. In contrast with the Primary and Sensory Motor Cortex regions, the main Visual Areas (ROIs **1, 181, 4, 184, 5, 185, 6, 186**) all lie below the fitted line.

If we consider the linear regression as signaling the mean performance between E_{LZ} and h_{LZ} , then our results can be interpreted that active visual regions underperform in terms of pattern generation for a given entropy density value, as their LZ-effective measure complexity falls below the regression line, and the active Primary Motor and Sensory cortex regions overperform under the same criteria. This motor exercise requires more precisely coordinated movement of fingers, toes and tongue, while visual attention can allow itself to be more loose as visual cues are given.

Other active areas on the left side of the threshold value are primarily involved in attentional processing and/or motor cue tasks. These include the previously described PGs (ROIs **151** and **331**) and PGi (ROIs **150** and **330**), which share many functions. The PFm Complex (ROIs **149** and **329**) plays a key role in attentional processing, decision-making, language syntax, and is activated in working memory, motor cues, and gambling tasks. The PF Complex (ROIs **148** and **328**) is primarily activated during motor cue and social Theory of Mind (ToM) tasks. Ventral Area 6 (ROIs **56** and **236**), part of the ventral secondary motor cortex, is associated with upper body movements (arms, neck, face, and mouth) when electrically stimulated. Additionally, Intra Parietal Area 1 (ROI **325**), which is also active in motor stimuli, has been consistently identified with interpreting motor cues, listening to stories, and mathematical problem solving, including mental arithmetic tasks and more active when processing faces than processing shapes^{38,40}.

A similar analysis can be made for the other task stimulus. During the motor, memory, and emotion tasks, subjects relied on visual cues to guide their actions, which corresponds to strong activation in visual regions across all three tasks. While visual areas are highly active in tasks with visual cues, they are less engaged in the language task, where the stimulus is auditory. Yet some differences may be relevant.

In the emotion task, 4.72% of the regions are active, namely: 1(181), 4(184), 5(185), 6(186), 18(198), 22(202), 69, 149(329), 151(331), 187, 325, 328, 330. The main visual areas overperformed with respect to the regression line, in contrast to the motor task. The emotional exercise involves recognizing faces and their emotional stand, the largest E_{LZ} values and smallest h_{LZ} values all correspond to the visual regions except the Fusiform Face Complex or FFC (ROI **198**) involved in face perception and identification, which plays a role in emotional expression recognition due to its high activity in response to both neutral and expressive faces (See⁴¹). For many years, it was believed that damage to this area was the cause of prosopagnosia⁴². Another paravisual area is the Inferior Temporal Cortex or PIT (ROIs **22** and **202**), which is involved in detecting faces and places. Area PIT is associated with processing fundamental aspects of color, such as hue, saturation, and brightness, using input from the eight visual area⁴³ or V8 (ROIs **7** and **187**), which is also active. The Inferior Temporal Cortex is a crucial component of the ventral visual pathway, contributing to the recognition of objects, faces, and scenes. It can be observed that this area shows high activity during the emotion tasks.

Several areas of attentional processing are activated during the emotion task, but many of them perform slightly below the regression line, though they are nearly on it. This applies to ROIs **151, 331, 149, 329, 148, 328, 150** and **330**, which were previously described in the motor task. In this context, attentional processing is not as critical or strongly linked to task performance as visual areas or face detection regions, which overperformed with respect to the regression line and showed higher activation in general.

Compare the active region in the emotion task with those in the memory task. In the memory exercise, 11.4% of the regions are active, namely: 1(181), 4(184), 5(185), 6(186), 7(187), 18(198), 21(201), 22(202), 138(318), 158(338), 200, 325, 329. Here, visual cues are also relevant, yet they are objects and neutral faces that are supposed not to convey emotions. The Fourth Visual Area or V4 (ROIs **6** and **186**) are still in the upper left region of the complexity-entropy map, yet the values of h_{LZ} have shifted towards lower values and, correspondingly, the E_{LZ} values have increased. Regions **185, 181** and **1**, all visual regions and clustered with ROIs **6** and **186** in the emotional task, are still strongly active in the memory exercise but are clearly separated from the last two. In the memory task both the visual regions and the object recognition areas lie close to the regression line and can not be considered under- or over-performing. The Inferior Temporal Cortex or PIT (ROI **22** and **202**) associated with the paravisual area is also strongly activated.

Area V3CD (ROIs **158** and **338**) is located between the early visual cortex and the MT complex. It is activated in fMRI scans during tasks involving tools, relational matching contrast, working memory, emotion, and place recognition. However, it shows less activation in body-related tasks and exhibits variable activation or deactivation in response to face-shape contrasts. Area V3CD combines detailed information about objects, including contrast and motion edges, to form a complete representation for recognizing objects⁴³. This area is highly activated, as expected, during the memory task.

The Lateral Occipital Cortex plays a key role in object processing, encoding, and recognition^{44,45}. The regions belonging to this cortex are Lateral Occipital areas 1, 2 and 3 or LO1 (ROIs **20** and **200**), LO2 (ROIs **21** and **201**), and LO3 (ROIs **159** and **339**). They are adjacent to areas PIT and V3CD, which are strongly activated during memory tasks involving object recognition and are located near the early visual cortex. We observed strong activation of LO1 and LO2 during memory tasks; but not of LO3, which is considered a new area in the Glasser study. LO3 has been shown to be more involved in the processing of the details, motion and shape information of objects⁴³.

In addition, the remaining active areas to be described are mostly paravision regions involved in processing the observed, specialized in object and face recognition, as previously mentioned, these include ROIs **18**, **198**, **7**, **187**, **325** and **138**), with the latter specifically associated with tool and place recognition^{37,43}. Additionally, attentional processing areas, such as ROIs **149** and **329** are also active.

In the language exercise, 13.61% of the regions are active, namely: 15(195), 69, 75, 125, 128, 131, 132, 144(324), 145(325), 149(329), 150(330), 176, 263, 268, 331. No visual cue is given, and accordingly, all areas associated with the visual regions do not appear activated in the complexity-entropy map. In contrast, areas associated with math are now strongly stimulated. The language exercise involves auditory cues and some regions of the auditory cortex have become active, such are the cases for the Superior Temporal Sulcus ventral anterior or STSva (ROIs **176**) and the Auditory Association Cortex (ROI **128**) which have not been activated in the other task exercise, and are mainly implicated in speech processing, specifically in the story-math contrast and in primary language tasks³⁷. The superior temporal sulcus (STS) is referred to by some authors as the "chameleon" of the human brain due to its involvement in a wide range of functions⁴⁶; in particular, the anterior region (STSva) is largely dedicated to speech processing.

In the language stimuli, Intra Parietal Areas 1 and 2 (IP1: ROIs **145** and **325**, and IP2: ROIs **144** and **324**) have consistently been implicated in tasks involving mathematical problem solving, showing significant activation during mental arithmetic tasks. Additionally, Area IP1 shows stronger activation in primary contrasts when interpreting motor cues and listening to a story, compared to when solving arithmetic problems^{38,40}. Correspondingly IP2 area (ROI **324**) shows the lowest h_{LZ} value and the strongest E_{LZ} values during the language stimulus but not in the other tasks. ROI **325**, strongly activated in the language task, also shows slight activation in the motor, memory, and emotion tasks, possibly due to its role in interpreting motor cues.

The area PGI (ROIs **150** and **330**) shows greater activity when listening to a story, especially compared to answering arithmetic problems, and also exhibits increased activation when processing faces³⁷. Additionally, this region becomes active when individuals shift their visuospatial attention from one location to another³⁸. These patterns are reflected in the entropic measures for language, where it is strongly activated. Additionally, this area shows strong activation in response to motor stimuli as well. The temporal area 1 anterior or TE1a (ROIs **132**) is more active in semantic pathways than visual pathways, showing greater activation during language processing tasks³⁷ and can be seen as active in the corresponding complexity-entropy map.

In the language exercise, the active regions can not be classified as under- or over-performing as they lie close to the linear regression fit.

For a better visualization of brain activity using entropy density, Figure 4 illustrates the activation levels of various brain regions during each stimulus, mapped onto the brain surface. The figure provides a detailed view of how different stimuli engage specific areas, highlighting the spatial distribution of neural activity. As previously discussed, lower values of h_{LZ} (represented in red) correspond to the most active regions involved in task processing, while higher h_{LZ} values (represented in blue) indicate lower activation levels. The exact locations of the discussed regions on the brain surface can be found in the supplementary material.

Notice how the tasks involving a visual cue, such as Motor, Memory and Emotion, show strong activation in the main visual areas located in the occipital lobe; this is not observed in the Language task, where the stimulus is auditory. Another notable pattern is the strong activation of the Motor and Sensory cortices, located in the posterior precentral gyrus, just anterior to the central sulcus, during the motor task in which the subject is asked to move their extremities; this activation is not present in the other tasks that are not focused on bodily movement.

On the other hand, we highlight the key role of the Face Fusiform Area (FFA) during the Emotion stimulus, where the subject observes faces to recognize emotions. This region is also active during the Memory task, although a bit weaker, as the visual attention is distributed across faces, places, tools, and body parts. In contrast, the FFA shows no activation during Motor and Language tasks, which do not involve facial stimuli.

Paravision areas involved in contrast, saturation, color detection, and, more generally, in the processing, encoding, and recognition of objects, such as the Inferior Temporal Cortex (PIT), Area PH, Occipital Scene Area (V3CD), and

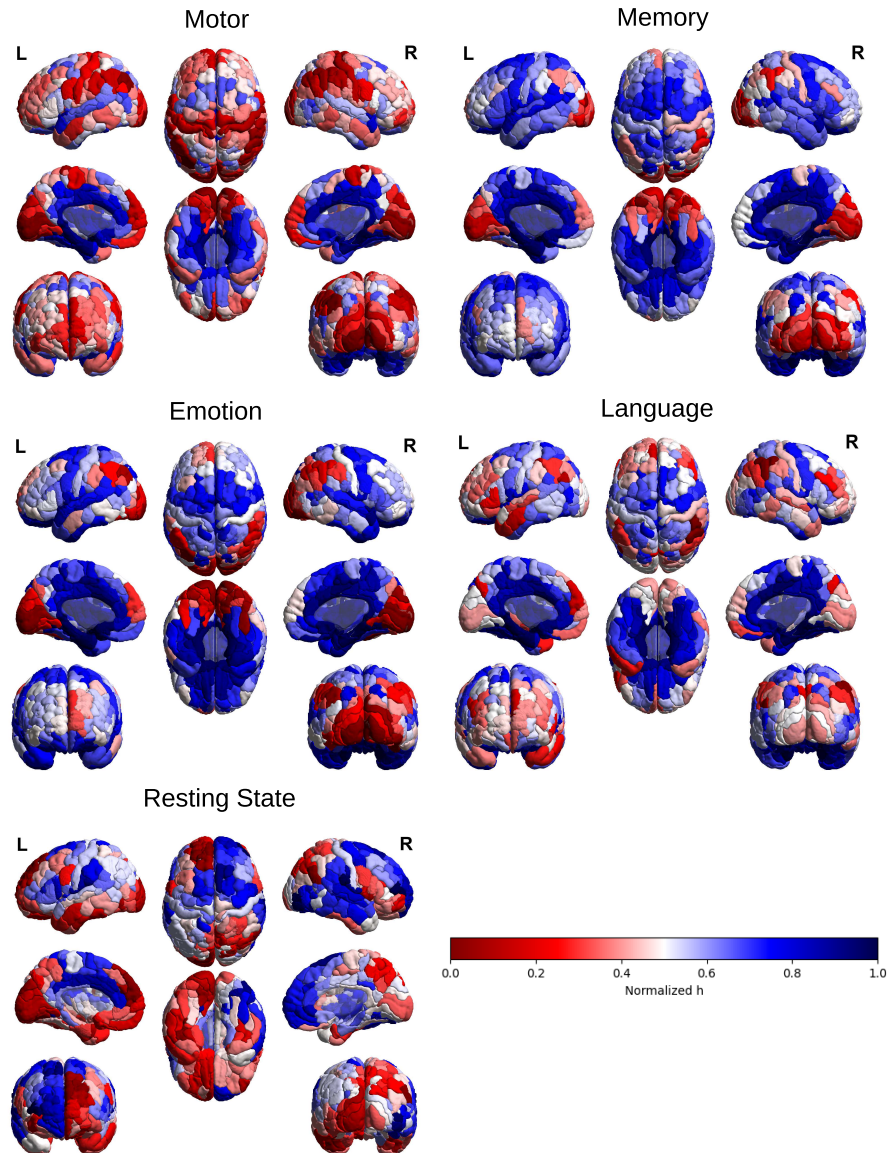


FIG. 4: **Brain mapping of activity levels.** Level of activation by the normalized entropy density in each stimulus. At lower h_{LZ} (red color) the regions are more active than at higher h_{LZ} (blue color). Notice how the visual regions in the occipital area are strongly activated during motor, emotion and memory stimuli, which have a visual cue. In contrast, during language stimuli, the visual areas are not active, but the auditory areas are. Observe the strong activation of the motor cortex in the posterior precentral gyrus, immediately anterior to the central sulcus, during the motor task but not in the others. Similarly, note the strong activation of the FFA and PIT -paraviscual areas specialized in face and object recognition, respectively- in the memory and emotion tasks, where faces are included in the stimuli; however, these areas are not active in the other tasks.

Lateral Occipital Cortex, are strongly activated during the Memory and Emotion stimuli, where subjects are engaged in recognizing and interpreting visual input. These regions are not active during the Language and Motor tasks, which do not require that level of visual processing.

The supplementary material can be consulted to locate the active regions involved in the Language task and to see how they are typically classified in the literature. These include Broca's areas, associated with language comprehension and production; mathematical processing areas, engaged during arithmetic problem-solving; and auditory regions, which are strongly activated during the Language task but not in response to the other stimuli.

The attentional processing areas identified in the supplementary material correspond to the previously described regions: PGs (ROIs **151** and **331**), PGi (ROIs **150** and **330**), PFm Complex (ROIs **149** and **329**), and PF Complex (ROIs **148** and **328**). These regions exhibit varying levels of activity across different stimuli.

In general, the motor regions are the 51.8%, 23.8%, 4.34%, and 5% of the active regions for the motor, emotion,

memory, and language, respectively, being the largest percent for the motor task, as should be expected. While the visual regions are the 29.6%, 57.1%, 96.6%, and 10% of the active regions for the motor, emotion, memory, and language, respectively, being maximum for the memory task, where it clearly plays a relevant role. In the language task, the language regions account for 65% of the active regions.

1. Areas that are identified as active in this study but are not typically considered activated

We look into regions found active in the complexity-entropy map, but not usually reported as active for the corresponding task.

Area 9m (ROIs **69**) is primarily located in the medial frontal lobe, and represents a more recent subdivision of the previously defined area 9 by Petrides and Pandya⁴⁷, which is a key part of the dorsolateral prefrontal cortex⁴⁸. This region exhibits increased activity when monitoring multiple pieces of spatial information. Compared to its superior neighbor, area 9p, area 9m is less deactivated (or more activated) in the language story contrast and displays stronger activation in the TOM-Random contrast³⁷. Although area 9m is not typically associated with language and algorithmic tasks, previous studies have indicated that it is less deactivated during the language story task. Our measures reveal strong activation in the language and motor exercises, along with slight activation in the memory, emotion tasks, potentially due to its role in monitoring multiple pieces of spatial information.

The Parieto-Occipital Sulcus area 2 or POS2 (ROI **195**) shows greater activation in the motor CUE-AVG contrast and reduced activation in the Face-AVG contrast, while it is more deactivated in the language, math, story, TOM-random, and faces-shapes contrasts, according to the study by Glasser et al. (2016)³⁷. However, in 2022, Matthew F. Glasser observed that this region demonstrated a relative preference for math⁴⁹; though they noted that math preferences may be confounded with auditory preferences in their data. The complexity-entropy map found strong activation in the language stimulus, where subjects were challenged with both story and math tasks.

The area 10v (ROIs **88** and **268**) is a newly identified ventral subregion of the preexisting area 10, which is one of the decision-making areas of the brain. This region contributes to behavioral decision-making by integrating information from the orbitofrontal cortex and the anterior cingulate cortex⁴⁸. In our entropic analysis, this region is highly activated during the motor task and slightly active in response to language stimuli.

Area 10d (ROIs **72**) is the dorsal subdivision of Area 10 and is involved in episodic and working memory tasks, contributing to abstract cognitive functions⁵⁰. This region shows strong activation during the complexity-entropy map of the motor task.

Intra Parietal Areas 1 (IP1: ROIs **325**) appear active in the emotion task, this area, as explained above is usually attached to abstract thinking such as mathematical operations (arithmetic tasks), and also when interpreting motor cues and listening to a story^{38,40}.

Area PGs (ROIs **331**) which have been reported active when individuals shift their visuospatial attention from one location to another, specifically in response to biological motion, are seen in the complexity-entropy map of the language task as activated even though there are no visual clues in this exercise.

It may surprise that regions of the hippocampus, parahippocampus, and amygdala are not included among active regions during memory stimuli, especially given the attention these areas have received in notable studies of patients with brain lesions, such as that of Henry Molaison⁵¹. In Molaison's case, episodic memory was affected due to the removal of these brain areas, while short-term memory remained intact⁵². Memory is a highly complex cognitive activity of many types. It is generally divided into long-term memory, which includes semantic, episodic, and procedural memory, among others; and short-term memory, which includes working memory. Working memory is characterized by the manipulation and active response to briefly stored information and is the type of memory of our current stimulus. Also, the amygdala and hippocampus are located beneath the cortical surface and are not directly represented in the Glasser atlas, which primarily focuses on the cerebral cortex⁵³.

2. The resting state as seen through the entropic magnitudes

During resting-state fMRI (rfMRI) scans, participants kept their eyes open, maintaining a relaxed fixation on a bright cross-hair projected onto a dark background in a dark room.

The resting state does not show the dispersion of values with respect to the linear regression fit, the threshold value as calculated for the specific task can not be performed, however, from the grouping of the low h_{LZ} points, 22 regions can be considered in the far left end of the plot as those more active. The active regions from the left hemisphere can be grouped, by physical continuity into three classes. The region with the lowest entropy density value and larger effective complexity measure is region 135(TF), belonging to the Temporal lobe, which together with its bordering neighboring regions 122(PeEc), 131(TE2a), 136(TE2p), all belonging also to the temporal lobe,

and the region 138(PH), belonging to the Occipital Lobe. A second border connected class is formed by regions 69(9m), 70(8BL), 71(9p), 72(10d), 86(9-46d) and 87(9a), all from the Lateral Front Lobe, which are also border connected to the active regions 62(d32), 88(10v), 91(11l) and 93(OFC). The third class of border connected active regions all belong to the Occipital Lobe and includes regions 1(V1), 4(V2) and 5(V3). In the right hemisphere, regions 225(0.29), 257(a47v), 258(6r), 315(TF), 330(PGi) appears active but have no border connection between them. The clear contrast between the more region activated left hemisphere and the less region activated right hemisphere, was evaluated using an asymmetry index. We computed the relative difference between hemisphere pairs for all 180 regions. The calculation involves taking the absolute value of the entropy density difference between both regions in a pair, and dividing it by the average value between them. Then the mean value over all relative difference is taken as the asymmetry index. The results corroborate the higher asymmetry between hemisphere in the resting state than in each specific task, the asymmetry index for the resting state was 0.41 while the same index gave the values 0.079, 0.078, 0.11 and 0.084 for the motor, emotion, language and memory experiments, respectively. From a functional perspective, the most represented functions of the active regions in the resting state are visual tasks with 11 regions, 8 regions with working memory, 8 regions with language processing, and 7 regions with movement. It must be recalled that the resting experiment was performed with eyes open focusing on a geometric object.

The largest E_{LZ} region in the resting state had been associated with memory (also face recognition, visual area, and language processing). The next region in terms of E_{LZ} value is 330(PGi) in the right hemisphere, related to language processing, attention, and mathematical tasks. These two regions are followed by the 69(9m) and 71(9p) regions, the first associated with the visual area and spatial information, and the latter with working memory. On the other side, the least activated regions, those with the largest h_{LZ} value, and the smaller E_{LZ} values are regions 201(LO2), 245(10r) and 327(PFop) on the right hemisphere.

A. Symmetry in the brain through subjects during tasks and asymmetry during Resting State

We observe a striking contrast between task-driven and resting-state brain dynamics, as shown in Figure 5 (Memory and Resting) and further supported by the supplementary figures for the other stimuli (Language, Motor, and Emotion). Specifically, all stimulus conditions exhibit a high degree of interhemispheric symmetry: homotopic regions across the left and right hemispheres display comparable levels of entropy density, suggesting coordinated bilateral activation. However, during the resting state, this symmetry is notably disrupted; entropy density diverges sharply between hemispheres, revealing a strong and widespread asymmetry. This breakdown of symmetry during rest is consistent with previous studies^{54–56} and highlights how, in the absence of external tasks, brain activity becomes more spontaneous and uneven between hemispheres.

B. Functional brain connections

To analyze the functional connections between brain regions, the LZ-distance was computed from the fMRI time series. Unlike Hamming-type distances, which assess similarity based on point-by-point matches, information distances aim to characterize the relationship between two time series via their normalized mutual information³³. In the case of the Lempel-Ziv estimate, this reflects the redundancy of patterns shared by the sequences. This redundancy-based measure is time-independent and does not account for when the related patterns occur in each series. While it is possible to assign a time arrow to information distances, this was not done in the present analysis and will be explored in future work. From the pairwise information distance between all 360 ROIs a distance matrix was computed. We plotted the distance map, sorting both axes by increasing h_{LZ} values. This matrix was then used to construct a dendrogram of the regions, enabling the definition of a hierarchical structure of functional relationships. The dendrogram was built using the Neighbor-Joining clustering method. Distance maps and dendrograms for all four tasks are shown in Figure 6.

Motor Task. We begin our analysis by the distance map, the larger the difference between the h_{LZ} value of two regions, the larger the distance between them. This trend is valid for both active and non-active regions. In general, the blue area color along the main diagonal shows that similar h_{LZ} valued regions remain close in the sense on pattern redundancy, but this diagonal area does not have the same width for all entropy density values and it reduces its width notably when entering the active regions portion of the distance map. The opposite happens for the less active regions portion of the same plot.

The first thing that becomes relevant in the dendrogram is that active regions are found clustered together at lower levels of the tree, pointing to shared information between them. Furthermore, regions of similar functionality also appeared clustered in the lower levels of the hierarchy. Both trends are clear, for example, for regions 1(V1), 181(V1), 5(V3), 185(V3), 6(V4), 186(V4), all of them in the occipital lobe and associated with visual tasks, which

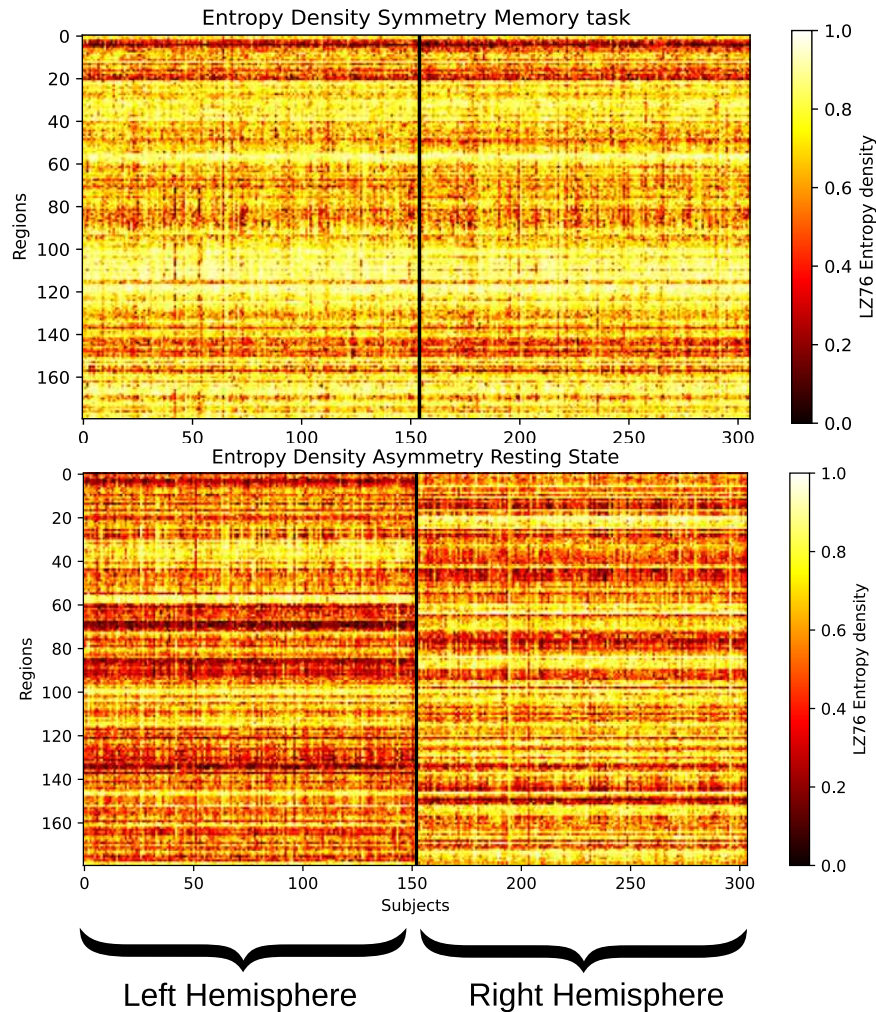


FIG. 5: **Symmetry and asymmetry across different tasks.** Both figures show the entropy density levels of each region across all subjects ($N = 153$). The left side displays regions in the left hemisphere (from 0 to 180), while the right side corresponds to the homologous regions in the right hemisphere (from 181 to 360). During task performance, a clear symmetry is observed between hemispheres, with homologous regions exhibiting similar activation levels. In contrast, this symmetry breaks down during the resting state, consistent with previous findings.⁵⁴

appear clustered together and also with the other visual area 4(V2), 184(V2), which although not activated according to the criteria used, has an entropy density of 0.83, quite close to the activation threshold value. A similar example are active regions 8(4), 188(4), 9(3b), 189(3b), 51(1), 231(1), 56(6v), 236(6v) all clustered together at low levels of the dendrogram and the first six regions associated with motor and sensory activity, while the last two belong to the premotor areas. A third more functionally heterogeneous group was also found comprising regions 6(V4), 72(10d), 148(PF), 328(PF), 149(PFm), 329(PFm), 150(PGi), 330(PGi), 151(PGs), 331(PGs), 325(IP1); the last nine regions belong to the lateral parietal lobe, while the first at the occipital lobe and the second at the lateral frontal lobe. This cluster comprises regions with visual, motor, and attention functionalities.

Emotion Task. A similar behavior was found in the emotional task, the distance map again shows that the larger the difference between the h_{LZ} value of two regions, the larger the distance between them. The dendrogram also shows the clustering of active regions. Now the active visual regions 1(V1), 4(V2), 5(V3), 6(V4) and their opposite hemisphere pair appear clustered at the leaf level. The same goes for regions 18(FFC) and 198(FFC) associated with emotional expression recognition, clustered together with regions 22(PIT) and 202(PIT), the four regions also associated with object recognition and visual functions. The ROI's 149(PFm), 151(PGs), and there opposite hemisphere pair, together with region 325(IP1) make another cluster related to attention functions. Regions 150(PGi) and 330(PGi) are also mentioned regarding emotional expression recognition. All these clusters are related at higher levels, forming a larger cluster, which did not happen in the motor task, where at least three separate clusters were found.

Memory Task. The memory task also has a large and unique group of active regions, mostly related to visual

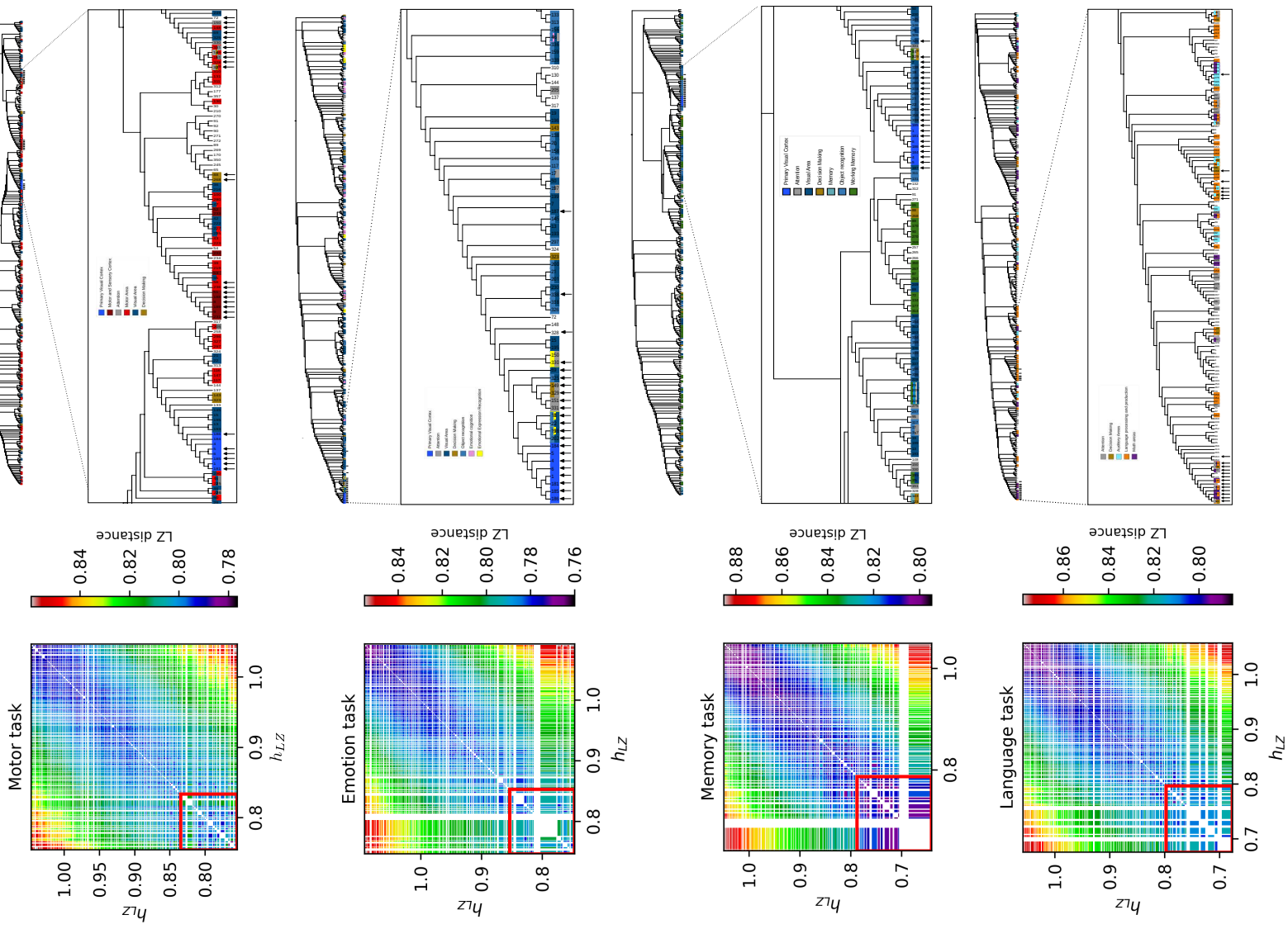


FIG. 6: **Distance analysis.** The Lempel Ziv distance was calculated between all brain regions, resulting in the distance matrix shown in Left. The matrix was rearranged based on activation levels, with lower h values indicating more active regions and higher h values indicating less active ones. The red square highlights the most active regions. As observed, active areas exhibit the greatest distance from non-active areas, while the non-active regions cluster closely together. This suggests that, despite appearing more random, they share underlying dynamics, potentially driven by a rewiring mechanism shaping their behavior. Right: A dendrogram was constructed from the distance matrix to illustrate hierarchical connections, showing clusters of visual, motor, and attentional processing regions, with strong associations among active regions.

functions and object recognition. All active Primary Visual Cortex regions appear together, regions 1(V1), 4(V2), 5(V3), 6(V4) and their opposite hemisphere pairs; at a higher hierarchy level they are clustered with regions 7(V8) and 187, 18(FFC) and 198, 21(LO2) and 201, 22(PIT) and 202, 138(PH) and 318, 158(V3CD) and 338(33pr), 200(LO1) all related to object recognition and visual area.

Language Task. Two well defined clusters of active regions can be recognized in the dendrogram. The first cluster with ROI's 15(POS2), 69(9m), 144(IP2), 145(IP1), 149(PFm), 150(PGi) and their opposite hemisphere pairs. All these regions have been reported to be associated with Language and mathematical tasks, as well as attention. The second cluster comprises regions active 128(STSda), 131(TGd), 132(TE1a), and 176(STSva), all associated with language processing and production, together with region 75(45).

IV. CONCLUSION

This study introduced a novel approach to identifying active brain regions in response to various stimuli using fMRI data. By applying entropy-based measures, we provide a robust framework to capture the intricate dynamics of brain activity, with a particular focus on detecting activation patterns through complexity metrics.

Our findings show that entropy is a valuable tool not only for identifying activation but also for capturing non-linear neural dynamics often missed by traditional linear methods. These metrics offer a richer understanding of the brain's complexity and its information-processing mechanisms.

Moreover, the results highlight the potential of entropic measures to quantify how information is transmitted between brain regions during task engagement. This paves the way for deeper exploration of brain function and dysfunction, with potential applications in both research and clinical contexts to advance our understanding of brain connectivity.

Due to the large volume of results obtained, this paper presents only the foundational findings, specifically, the characterization of brain activations using entropy density. These results serve as a consistency check, confirming that entropic measures can reliably reflect brain activity. Building on this foundation, a forthcoming paper will present a more in-depth analysis of functional brain connectivity using Lempel-Ziv distance, an information-theoretic measure designed to detect associations and causal relationships. That work will focus on how brain regions interact, coordinate, and transmit information during cognitive tasks.

Finally, the consistency of our findings across multiple stimuli, validated through dendrogram-based comparisons, reinforces the utility of entropy-based methods in both research and clinical contexts for advancing the understanding of brain connectivity.

V. ACKNOWLEDGEMENTS

CITMA is acknowledged for financial support under the project CARDENT, grant PN223LH010-053. Kárel García and Roberto Bernal Arencibia are acknowledged for valuable discussions. The University of Havana and Max Planck Institute for the Physics of Complex Systems are acknowledged for their computer support and working environment. JS Armand Eyebe Fouda is acknowledged for valuable discussions, particularly regarding the creation of Figure 5.

VI. FINANCIAL DISCLOSURE

This research received no external funding.

VII. CONFLICT OF INTEREST

The authors declare no potential conflict of interest.

¹ Larry W. Swanson and Jeff W. Lichtman. From Cajal to Connectome and Beyond. 39(1):197–216, 2016. ISSN 0147-006X, 1545-4126. doi: 10.1146/annurev-neuro-071714-033954.

² Andreas Spiegler, Jens Haueisen, Thomas R. Knösche, and Viktor K. Jirsa. *Dynamics of Biologically Informed Neural Mass Models of the Brain*. Univ.-Verl. Ilmenau, 2012. ISBN 978-3-86360-024-2.

- ³ Lianne H. Scholtens, Rory Pijnenburg, Siemon C. De Lange, Inge Huitinga, Martijn P. Van Den Heuvel, and Netherlands Brain Bank. Common Microscale and Macroscale Principles of Connectivity in the Human Brain. 42(20):4147–4163, 2022. ISSN 0270-6474, 1529-2401. doi: 10.1523/JNEUROSCI.1572-21.2022.
- ⁴ Martijn P. Van Den Heuvel, Lianne H. Scholtens, Lisa Feldman Barrett, Claus C. Hilgetag, and Marcel A. De Reus. Bridging Cytoarchitectonics and Connectomics in Human Cerebral Cortex. 35(41):13943–13948, 2015. ISSN 0270-6474, 1529-2401. doi: 10.1523/JNEUROSCI.2630-15.2015.
- ⁵ Meichen Yu, Olaf Sporns, and Andrew J. Saykin. The human connectome in Alzheimer disease — relationship to biomarkers and genetics. 17(9):545–563, 2021. ISSN 1759-4758, 1759-4766. doi: 10.1038/s41582-021-00529-1.
- ⁶ Tianyi Yan, Wenhui Wang, Liu Yang, Kewei Chen, Rong Chen, and Ying Han. Rich club disturbances of the human connectome from subjective cognitive decline to Alzheimer’s disease. 8(12):3237–3255, 2018. ISSN 1838-7640. doi: 10.7150/thno.23772.
- ⁷ Arianna Bellucci, Nicola Biagio Mercuri, Annalena Venneri, Gaia Faustini, Francesca Longhena, Marina Pizzi, Cristina Missale, and PierFranco Spano. Review: Parkinson’s disease: From synaptic loss to connectome dysfunction. 42(1):77–94, 2016. ISSN 0305-1846, 1365-2990. doi: 10.1111/nan.12297.
- ⁸ Michael D. Fox. Mapping Symptoms to Brain Networks with the Human Connectome. 379(23):2237–2245, 2018. ISSN 0028-4793, 1533-4406. doi: 10.1056/NEJMra1706158.
- ⁹ Roberto Cabeza and Lars Nyberg. Imaging cognition ii: An empirical review of 275 pet and fmri studies. *Journal of Cognitive Neuroscience*, 12(1):1–47, 01 2000. ISSN 0898-929X. doi: 10.1162/08989290051137585. URL <https://doi.org/10.1162/08989290051137585>.
- ¹⁰ Debra A Gusnard and Marcus E Raichle. Searching for a baseline: functional imaging and the resting human brain. *Nature reviews neuroscience*, 2(10):685–694, 2001.
- ¹¹ Joseph R Simpson Jr, Abraham Z Snyder, Debra A Gusnard, and Marcus E Raichle. Emotion-induced changes in human medial prefrontal cortex: I. during cognitive task performance. *Proceedings of the National Academy of Sciences*, 98(2):683–687, 2001.
- ¹² Maurizio Corbetta and Gordon L Shulman. Control of goal-directed and stimulus-driven attention in the brain. *Nature reviews neuroscience*, 3(3):201–215, 2002.
- ¹³ Pedro A. Valdes-Sosa, Alard Roebroeck, Jean Daunizeau, and Karl Friston. Effective connectivity: Influence, causality and biophysical modeling. 58(2):339–361, 2011. ISSN 10538119. doi: 10.1016/j.neuroimage.2011.03.058.
- ¹⁴ Natalia Z. Bielczyk, Fabian Walocha, Patrick W. Ebel, Koen V. Haak, Alberto Llera, Jan K. Buitelaar, Jeffrey C. Glennon, and Christian F. Beckmann. Thresholding functional connectomes by means of mixture modeling. 171:402–414, 2018. ISSN 10538119. doi: 10.1016/j.neuroimage.2018.01.003.
- ¹⁵ Lionel Barnett and Anil K. Seth. Granger causality for state space models. 91(4):040101, 2015. ISSN 1539-3755, 1550-2376. doi: 10.1103/PhysRevE.91.040101.
- ¹⁶ M. J. Kaminski and K. J. Blinowska. A new method of the description of the information flow in the brain structures. 65(3):203–210, 1991. ISSN 0340-1200, 1432-0770. doi: 10.1007/BF00198091.
- ¹⁷ Luiz A. Baccalá and Koichi Sameshima. Partial directed coherence: A new concept in neural structure determination. 84(6):463–474, 2001. ISSN 0340-1200. doi: 10.1007/PL00007990.
- ¹⁸ Ed Bullmore and Olaf Sporns. Complex brain networks: Graph theoretical analysis of structural and functional systems. 10(3):186–198, 2009. ISSN 1471-003X, 1471-0048. doi: 10.1038/nrn2575.
- ¹⁹ Teddy J. Akiki and Chadi G. Abdallah. Determining the Hierarchical Architecture of the Human Brain Using Subject-Level Clustering of Functional Networks. 9(1):19290, 2019. ISSN 2045-2322. doi: 10.1038/s41598-019-55738-y.
- ²⁰ D.C. Van Essen, K. Ugurbil, E. Auerbach, D. Barch, T.E.J. Behrens, R. Bucholz, A. Chang, L. Chen, M. Corbetta, S.W. Curtiss, S. Della Penna, D. Feinberg, M.F. Glasser, N. Harel, A.C. Heath, L. Larson-Prior, D. Marcus, G. Michalareas, S. Moeller, R. Oostenveld, S.E. Petersen, F. Prior, B.L. Schlaggar, S.M. Smith, A.Z. Snyder, J. Xu, and E. Yacoub. The Human Connectome Project: A data acquisition perspective. 62(4):2222–2231, 2012. ISSN 10538119. doi: 10.1016/j.neuroimage.2012.02.018.
- ²¹ Yang Tian, Guoqi Li, and Pei Sun. Bridging the information and dynamics attributes of neural activities. 3(4):043085, 2021. ISSN 2643-1564. doi: 10.1103/PhysRevResearch.3.043085.
- ²² Ze Wang, Yin Li, Anna Rose Childress, and John A. Detre. Brain Entropy Mapping Using fMRI. 9(3):e89948. ISSN 1932-6203. doi: 10.1371/journal.pone.0089948.
- ²³ Temujin Gautama, Danilo P. Mandic, and Marc M. Van Hulle. Indications of nonlinear structures in brain electrical activity. 67(4):046204, 2003. ISSN 1063-651X, 1095-3787. doi: 10.1103/PhysRevE.67.046204.
- ²⁴ Thomas M Cover and Joy A Thomas. *Elements of information theory*. John Wiley & Sons, 1999.
- ²⁵ P. Grassberger. Towards a quantitative theory of self-generated complexity. *Int. J. Theo. Phys.*, 25:907–938, 1986.
- ²⁶ James P. Crutchfield and David P. Feldman. Regularities unseen, randomness observed: Levels of entropy convergence. 13(1):25–54, 2003. ISSN 1054-1500, 1089-7682. doi: 10.1063/1.1530990.
- ²⁷ Ernesto Estevez-Rams, Ania Mesa-Rodriguez, and Daniel Estevez-Moya. Complexity-entropy analysis at different levels of organisation in written language. 14(5):e0214863, 2019. ISSN 1932-6203. doi: 10.1371/journal.pone.0214863.
- ²⁸ Wu-Minn and HCP. 1200 subjects data release reference manual. 565:213, 2017.
- ²⁹ Matthew F. Glasser, Stamatis N. Sotiropoulos, J. Anthony Wilson, Timothy S. Coalson, Bruce Fischl, Jesper L. Andersson, Junqian Xu, Saad Jbabdi, Matthew Webster, Jonathan R. Polimeni, David C. Van Essen, and Mark Jenkinson. The minimal preprocessing pipelines for the Human Connectome Project. 80:105–124, 2013. ISSN 10538119. doi: 10.1016/j.neuroimage.2013.04.127.
- ³⁰ A. Lesne, J.L.Blanc, and L. Pezard. Entropy estimation of very short symbolic sequences. *Phys. Rev. E*, 79:046208–046217,

- 2009.
- 31 O. Melchert and A. K. Hartmann. Analysis of the phase transition in the two-dimensional ising ferromagnet using a lempel-ziv string-parsing scheme and black-box data-compression utilities. *Phys. Rev. E*, 91:023306–023317, 2015.
 - 32 E. Estevez-Rams, D. Estevez-Moya, K. Garcia-Medina, and R. Lora-Serrano. Computational capabilities at the edge of chaos for one dimensional systems undergoing continuous transitions. *Chaos*, 29:043105, 2019.
 - 33 M. Li, X. Chen, X. Li, B. Ma, and P. M. B. Vitanyi. The similarity metric. *IEEE Trans. Inf. Th.*, 50:3250–3264, 2004.
 - 34 A. N. Kolmogorov. Three approaches to the concept of the amount of information. *Probl. Inf. Transm. (English Trans.)*, 1:1–7, 1965.
 - 35 E. Estevez-Rams, R. Lora-Serrano, C. A. J. Nunes, and B. Aragón-Fernández. Lempel-Ziv complexity analysis of one dimensional cellular automata. *Chaos*, 25:123106–123116, 2015.
 - 36 Takuya Ito, Scott L. Brincat, Markus Siegel, Ravi D. Mill, Biyu J. He, Earl K. Miller, Horacio G. Rotstein, and Michael W. Cole. Task-evoked activity quenches neural correlations and variability across cortical areas. 16(8):e1007983, 2020. ISSN 1553-7358. doi: 10.1371/journal.pcbi.1007983.
 - 37 Matthew F. Glasser, Timothy S. Coalson, Emma C. Robinson, Carl D. Hacker, John Harwell, Essa Yacoub, Kamil Ugurbil, Jesper Andersson, Christian F. Beckmann, Mark Jenkinson, Stephen M. Smith, and David C. Van Essen. A multi-modal parcellation of human cerebral cortex. 536(7615):171–178, 2016. ISSN 0028-0836, 1476-4687. doi: 10.1038/nature18933.
 - 38 Cordell M Baker, Joshua D Burks, Robert G Briggs, Andrew K Conner, Chad A Glenn, Kathleen N Taylor, Goksel Sali, Tressie M McCoy, James D Battiste, Daniel L O’Donoghue, and Michael E Sughrue. A Connectomic Atlas of the Human Cerebrum—Chapter 7: The Lateral Parietal Lobe. 15:S295–S349, 2018. ISSN 2332-4252, 2332-4260. doi: 10.1093/ons/opy261.
 - 39 Cordell M Baker, Joshua D Burks, Robert G Briggs, John R Sheets, Andrew K Conner, Chad A Glenn, Goksel Sali, Tressie M McCoy, James D Battiste, Daniel L O’Donoghue, and Michael E Sughrue. A Connectomic Atlas of the Human Cerebrum—Chapter 3: The Motor, Premotor, and Sensory Cortices. 15:S75–S121, 2018. ISSN 2332-4252, 2332-4260. doi: 10.1093/ons/opy256.
 - 40 S. S. Wu, T. T. Chang, A. Majid, S. Caspers, S. B. Eickhoff, and V. Menon. Functional Heterogeneity of Inferior Parietal Cortex during Mathematical Cognition Assessed with Cytoarchitectonic Probability Maps. 19(12):2930–2945, 2009. ISSN 1047-3211, 1460-2199. doi: 10.1093/cercor/bhp063.
 - 41 Xiayu Chen, Xingyu Liu, Benjamin J. Parker, Zonglei Zhen, and Kevin S. Weiner. Functionally and structurally distinct fusiform face area(s) in over 1000 participants. 265:119765, 2023. ISSN 10538119. doi: 10.1016/j.neuroimage.2022.119765.
 - 42 Jennifer K.E. Steeves, Jody C. Culham, Bradley C. Duchaine, Cristiana Cavina Pratesi, Kenneth F. Valyear, Igor Schindler, G. Keith Humphrey, A. David Milner, and Melvyn A. Goodale. The fusiform face area is not sufficient for face recognition: Evidence from a patient with dense prosopagnosia and no occipital face area. 44(4):594–609, 2006. ISSN 00283932. doi: 10.1016/j.neuropsychologia.2005.06.013.
 - 43 Cordell M Baker, Joshua D Burks, Robert G Briggs, Jordan Stafford, Andrew K Conner, Chad A Glenn, Goksel Sali, Tressie M McCoy, James D Battiste, Daniel L O’Donoghue, and Michael E Sughrue. A Connectomic Atlas of the Human Cerebrum—Chapter 9: The Occipital Lobe. 15:S372–S406, 2018. ISSN 2332-4252, 2332-4260. doi: 10.1093/ons/opy263.
 - 44 Kalanit Grill-Spector, Zoe Kourtzi, and Nancy Kanwisher. The lateral occipital complex and its role in object recognition. 41(10-11):1409–1422, 2001. ISSN 00426989. doi: 10.1016/S0042-6989(01)00073-6.
 - 45 R Malach, J B Reppas, R R Benson, K K Kwong, H Jiang, W A Kennedy, P J Ledden, T J Brady, B R Rosen, and R B Tootell. Object-related activity revealed by functional magnetic resonance imaging in human occipital cortex. 92(18): 8135–8139, 1995. ISSN 0027-8424, 1091-6490. doi: 10.1073/pnas.92.18.8135.
 - 46 Grit Hein and Robert T. Knight. Superior Temporal Sulcus—It’s My Area: Or Is It? 20(12):2125–2136. ISSN 0898-929X, 1530-8898. doi: 10.1162/jocn.2008.20148.
 - 47 Michael Petrides and DN Pandya. Dorsolateral prefrontal cortex: comparative cytoarchitectonic analysis in the human and the macaque brain and corticocortical connection patterns. *European journal of neuroscience*, 11(3):1011–1036, 1999.
 - 48 Cordell M Baker, Joshua D Burks, Robert G Briggs, Jordan Stafford, Andrew K Conner, Chad A Glenn, Goksel Sali, Tressie M McCoy, James D Battiste, Daniel L O’Donoghue, and Michael E Sughrue. A Connectomic Atlas of the Human Cerebrum—Chapter 4: The Medial Frontal Lobe, Anterior Cingulate Gyrus, and Orbitofrontal Cortex. 15:S122–S174, 2018. ISSN 2332-4252, 2332-4260. doi: 10.1093/ons/opy257.
 - 49 Moataz Assem, Matthew F Glasser, David C Van Essen, and John Duncan. A Domain-General Cognitive Core Defined in Multimodally Parcellated Human Cortex. 30(8):4361–4380, 2020. ISSN 1047-3211, 1460-2199. doi: 10.1093/cercor/bhaa023.
 - 50 Cordell M Baker, Joshua D Burks, Robert G Briggs, Andrew K Conner, Chad A Glenn, Jake P Morgan, Jordan Stafford, Goksel Sali, Tressie M McCoy, James D Battiste, Daniel L O’Donoghue, and Michael E Sughrue. A Connectomic Atlas of the Human Cerebrum—Chapter 2: The Lateral Frontal Lobe. 15:S10–S74, 2018. ISSN 2332-4252, 2332-4260. doi: 10.1093/ons/opy254.
 - 51 Rimal Hanif Dossani, Symeon Missios, and Anil Nanda. The legacy of henry molaison (1926–2008) and the impact of his bilateral mesial temporal lobe surgery on the study of human memory. *World neurosurgery*, 84(4):1127–1135, 2015.
 - 52 Howard Eichenbaum. *The cognitive neuroscience of memory: An introduction*. Oxford University Press, 2011.
 - 53 Robert G Briggs, Andrew K Conner, Meherzad Rahimi, Goksel Sali, Cordell M Baker, Joshua D Burks, Chad A Glenn, James D Battiste, and Michael E Sughrue. A Connectomic Atlas of the Human Cerebrum—Chapter 14: Tractographic Description of the Frontal Aslant Tract. 15:S444–S449, 2018. ISSN 2332-4252, 2332-4260. doi: 10.1093/ons/opy268.
 - 54 Mathijs Raemaekers, Wouter Schellekens, Natalia Petridou, and Nick F. Ramsey. Knowing left from right: Asymmetric functional connectivity during resting state. 2018. ISSN 1863-2653, 1863-2661. doi: 10.1007/s00429-017-1604-y.
 - 55 Bin Wang, Lan Yang, Wenjie Yan, Weichao An, Jie Xiang, and Dandan Li. Brain asymmetry: A novel perspective on

hemispheric network. 9(2):56–77, 2023. ISSN 2096-5958, 2096-5958. doi: 10.26599/BSA.2023.9050014.

⁵⁶ Victor M. Saenger, Fernando A. Barrios, María L. Martínez-Gudiño, and Sarael Alcauter. Hemispheric asymmetries of functional connectivity and grey matter volume in the default mode network. 50(7):1308–1315, 2012. ISSN 00283932. doi: 10.1016/j.neuropsychologia.2012.02.014.

⁵⁷ E. Estevez-Rams, R. Lora-Serrano, C. A. J. Nunes, and B. Aragón-Fernández. Lempel-Ziv complexity analysis of one dimensional cellular automata. 25(12):123106, 2015. ISSN 1054-1500, 1089-7682. doi: 10.1063/1.4936876.

⁵⁸ J. Ziv. Coding theorems for individual sequences. 24(4):405–412, 1978. ISSN 0018-9448. doi: 10.1109/TIT.1978.1055911.

VIII. SUPPLEMENTARY MATERIAL

A. Lempel-Ziv Complexity

The Lempel-Ziv Complexity is introduced due to the difficulty of estimating the Entropy Density for finite-length sequences. Its definition is based on a specific factorization of a sequence, adding a new factor whenever a new pattern appears.

A factorization of a sequence S of length N is defined as its partition into disjoint blocks:

$$F(S) = S(1, l_1), S(l_1 + 1, l_2), S(l_2 + 1, l_3), \dots, S(l_{m-1} + 1, N)$$

The factorization $F(S)$ is called the Lempel-Ziv factorization or exhaustive history if each factor $S(l_{k-1} + 1, l_k)$ is not a substring of the string $S(1, l_k - 1)$, while $S(l_{k-1} + 1, l_k - 1)$ is a substring of $S(1, l_k - 2)$

The exhaustive history is unique for each sequence⁵⁷, allowing us to define the Lempel-Ziv complexity of the sequence S , denoted as $C_{LZ}(S)$, as the number of factors in its exhaustive history.

For example, given the sequence $S = 11011101000011$, its exhaustive history is $F(S) = 1.10.111.010.0001.1$, where each factor is delimited by a dot. This factorization contains 6 elements, so $C_{LZ}(S) = 6$.

Jacob Ziv demonstrated that if S is the output of an ergodic process with Entropy Density $h_\mu(S)$, then the following holds⁵⁸:

$$\overline{\lim}_{N \rightarrow \infty} \frac{C_{LZ}(S)}{N / \log N} = h_\mu(S) \quad (3)$$

Equation (3) is valid in the infinite limit; however, in practice, it is used as an estimate of the Entropy Density.

From a computational point of view, it is advantageous to use C_{LZ} to estimate the Entropy Density when $N \gg 1$, as the Lempel-Ziv complexity is algorithmically computable.

B. Threshold selection criterion

The criterion for selecting the threshold was based on the maximum fitting error observed when approximating each point and its ten nearest neighbors (in the h_{LZ} regime) to a linear curve. This error reflects the point at which the scatter begins to deviate significantly from the fitted line on average. This behavior is illustrated in Figure 7.

C. Location of key regions on the brain surface

To better understand the Figure 4, we include the following image to indicate the locations of the referenced regions on the brain surface.

D. Symmetry across different tasks

To complement the main analysis shown in Figure 5, we include here the remaining tasks: Language, Motor, and Emotion, to illustrate the consistency of the observed interhemispheric symmetry across all stimulus conditions. As in the Memory task, these additional cases confirm that task-driven brain activity elicits a strong bilateral pattern, with homotopic regions in both hemispheres displaying similar entropy density levels. This supplementary figure further supports the contrast with the resting state, where symmetry breaks down and widespread asymmetry emerges.

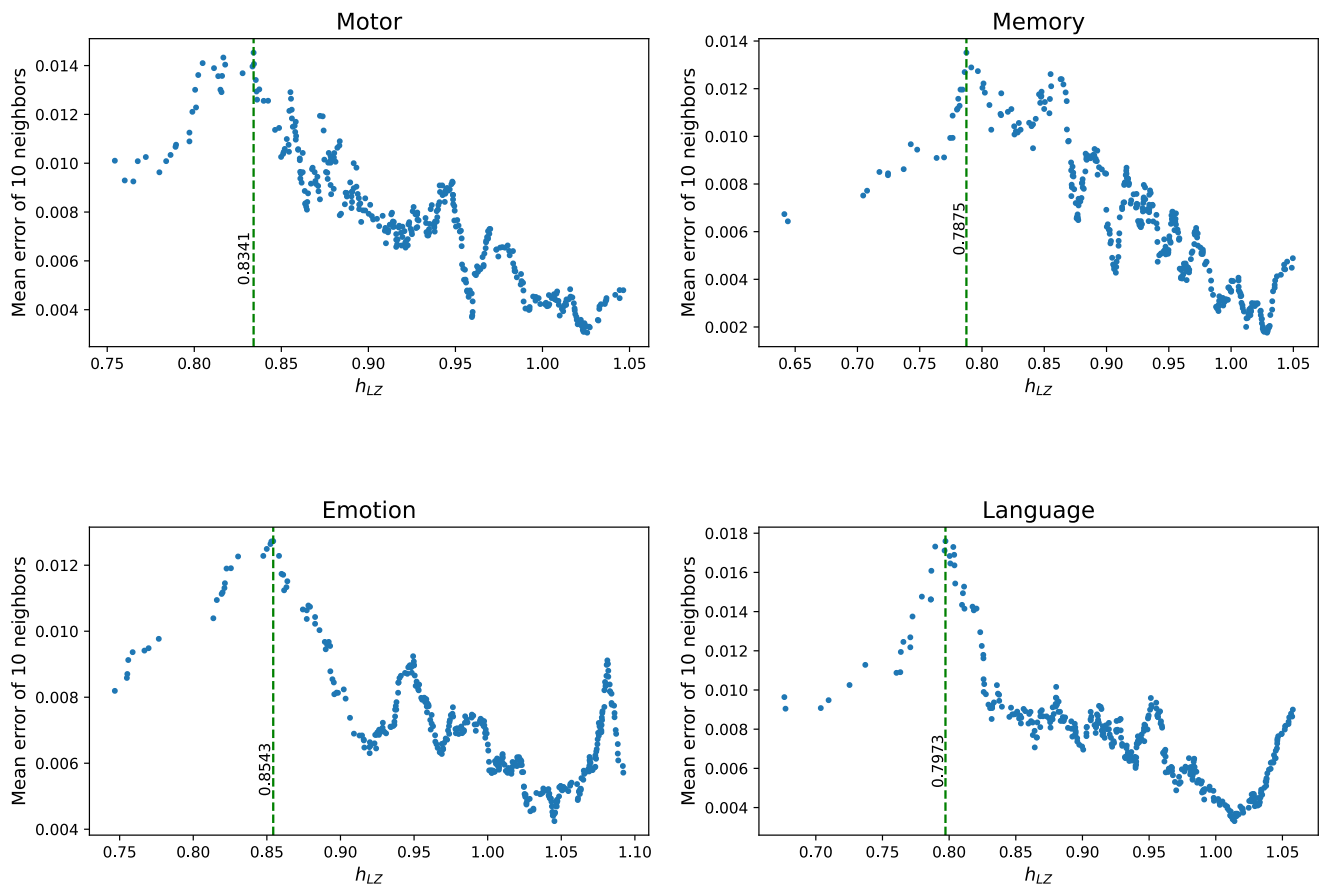


FIG. 7: **Criterion of active regions.** A linear fit was computed from the complexity map. The mean residual was calculated for each point and its ten nearest neighbors and plotted as a function of h_{LZ} . The threshold was selected as the maximum in the plot where the scatter significantly deviates from the line on average.

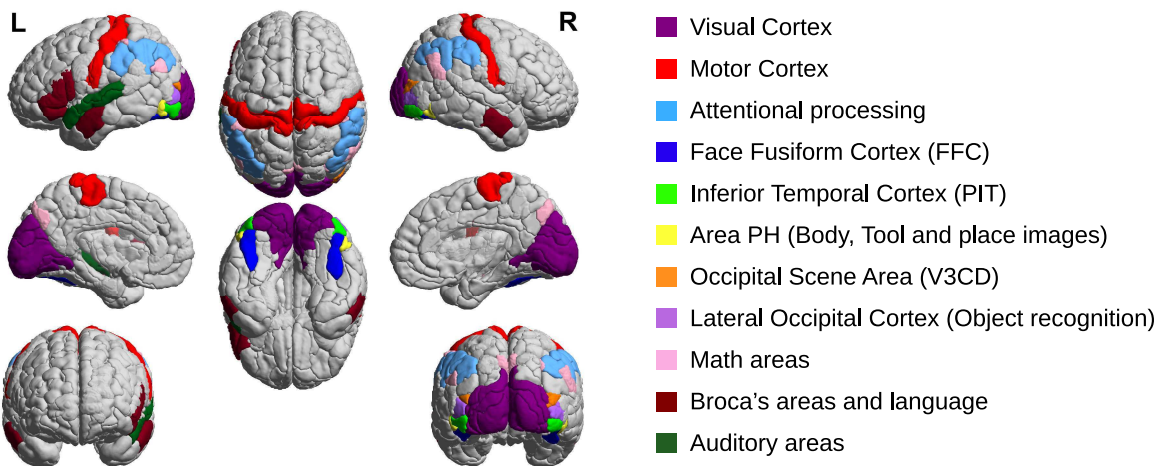


FIG. 8: **Brain regions location.** Visualization of the brain surface with labeled regions of interest (ROIs) referenced in Figure 4

E. Comparison of active brain regions with previous studies

Task	Common in previous and our work	Reported in previous studies	Reported in our work
Motor	1, 4, 5, 6, 8, 9, 51, 52, 53, 56, 148, 149, 150, 151, 181, 184, 185, 186, 188, 189, 231, 232, 233, 236, 328, 329, 330, 331	10, 11, 12, 26, 36, 37, 39, 44, 54, 55, 78, 96, 190, 191, 192, 206, 216, 217, 219, 224, 234, 235, 258, 276	69, 72, 88, 132, 249, 257, 268, 325
Memory	1, 4, 5, 6, 7, 18, 20, 21, 22, 138, 149, 158, 181, 184, 185, 186, 187, 198, 200, 201, 202, 263, 318, 329, 338	2, 15, 27, 29, 30, 31, 46, 65, 72, 83, 84, 85, 86, 89, 90, 121, 133, 134, 136, 138, 141, 142, 143, 155, 156, 157, 158, 170, 177, 182, 195, 207, 209, 210, 211, 226, 245, 252, 264, 265, 266, 269, 270, 301, 313, 314, 316, 318, 321, 322, 323, 335, 336, 337, 338, 350, 357	69, 325, 326
Emotion	1, 4, 5, 6, 18, 22, 181, 184, 185, 186, 198, 202	7, 18, 66, 91, 92, 93, 94, 128, 129, 130, 153, 154, 160, 163, 166, 176, 187, 198, 243, 246, 271, 272, 273, 274, 308, 309, 310, 333, 334, 340, 346, 356	69, 149, 151, 325, 329, 328, 330, 331
Language	75, 76, 125, 128, 129, 130, 132, 144, 145, 176, 305, 324, 325, 356	12, 24, 25, 26, 74, 96, 104, 107, 123, 124, 150, 173, 174, 175, 204, 276, 284, 303, 304, 307, 308, 309, 310, 330, 353, 354, 355	15, 63, 69, 83, 131, 149, 150, 195, 264, 265, 268, 329, 330, 331

TABLE I: Active regions for each stimulus, overlapping and new findings in comparison with other studies. Brain regions commonly found in other studies and areas uniquely active in our analysis, showing both overlap and new findings.

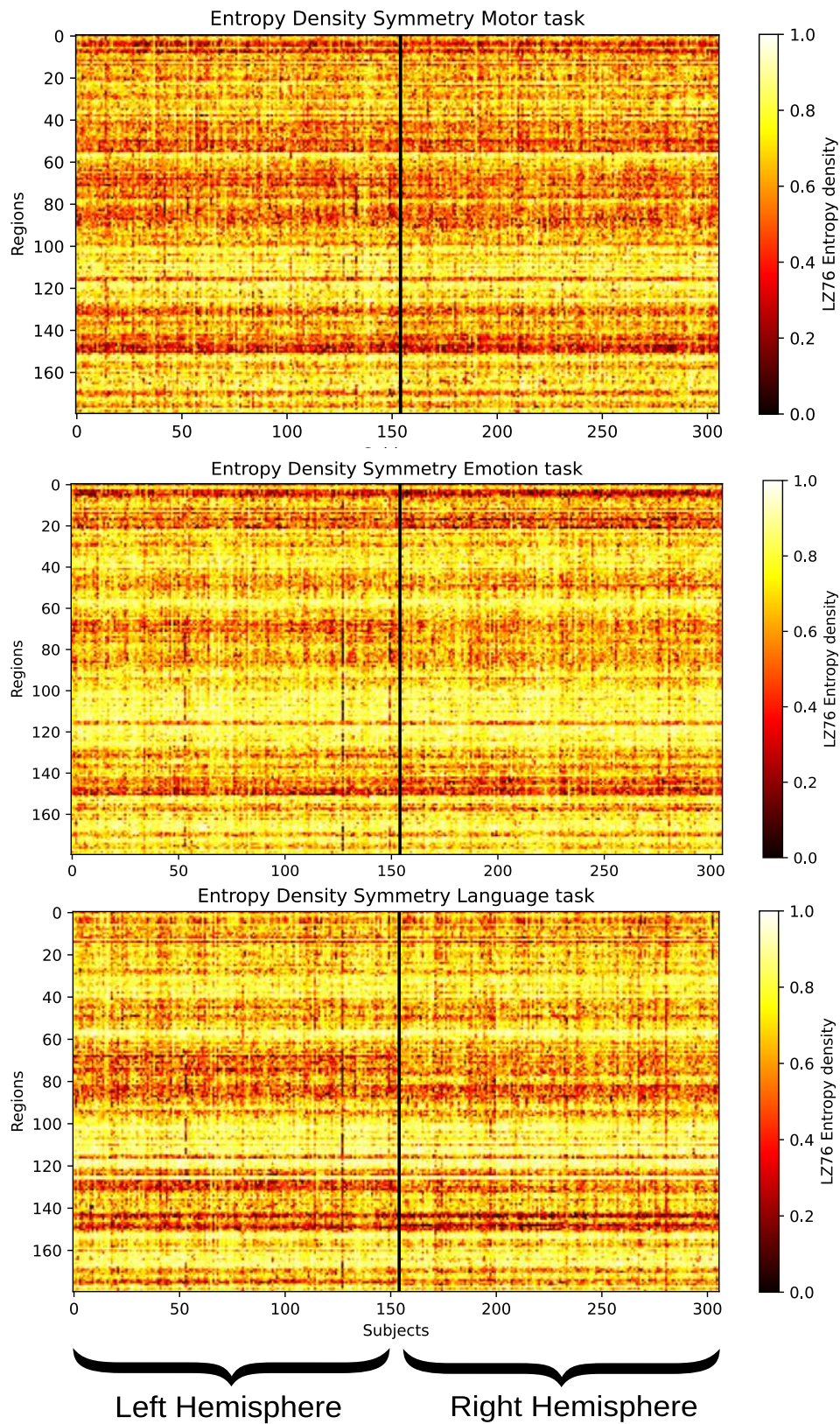


FIG. 9: **Symmetry across different tasks.** The figure shows the entropy density levels of each region across all subjects ($N = 153$). The left side displays regions in the left hemisphere (from 0 to 180), while the right side corresponds to the homologous regions in the right hemisphere (from 181 to 360). During each task performance, a clear symmetry is observed between hemispheres, with homologous regions exhibiting similar activation levels.